The ISME Journal (2016) 10, 1742–1754

www.nature.com/ismej

ORIGINAL ARTICLE

Modulation of host ROS metabolism is essential for viral infection of a bloom-forming coccolithophore in the ocean

Uri Sheyn[1], Shilo Rosenwasser[1], Shifra Ben-Dor[2], Ziv Porat[2] and Assaf Vardi[1]
[1]*Department of Plant and Environmental Sciences, Weizmann Institute of Science, Rehovot, Israel and*
[2]*Department of Biological Services, Weizmann Institute of Science, Rehovot, Israel*

The cosmopolitan coccolithophore *Emiliania huxleyi* is a unicellular eukaryotic alga responsible for vast blooms in the ocean. These blooms have immense impact on large biogeochemical cycles and are terminated by a specific large double-stranded DNA *E. huxleyi* virus (EhV, *Phycodnaviridae*). EhV infection is accompanied by induction of hallmarks of programmed cell death and production of reactive oxygen species (ROS). Here we characterized alterations in ROS metabolism and explored its role during infection. Transcriptomic analysis of ROS-related genes predicted an increase in glutathione (GSH) and H_2O_2 production during infection. In accordance, using biochemical assays and specific fluorescent probes we demonstrated the overproduction of GSH during lytic infection. We also showed that H_2O_2 production, rather than superoxide, is the predominant ROS during the onset of the lytic phase of infection. Using flow cytometry, confocal microscopy and multispectral imaging flow cytometry, we showed that the profound co-production of H_2O_2 and GSH occurred in the same subpopulation of cells but at different subcellular localization. Positively stained cells for GSH and H_2O_2 were highly infected compared with negatively stained cells. Inhibition of ROS production by application of a peroxidase inhibitor or an H_2O_2 scavenger inhibited host cell death and reduced viral production. We conclude that viral infection induced remodeling of the host antioxidant network that is essential for a successful viral replication cycle. This study provides insight into viral replication strategy and suggests the use of specific cellular markers to identify and quantify the extent of active viral infection during *E. huxleyi* blooms in the ocean.
The ISME Journal (2016) **10,** 1742–1754; doi:10.1038/ismej.2015.228; published online 19 January 2016

Introduction

Phytoplankton blooms are of immense ecological importance, as they serve as the foundation for marine food webs, are major sinks for atmospheric CO_2 and are responsible for approximately half of the primary productivity on Earth (Field *et al.*, 1998; Behrenfeld *et al.*, 2006). Opposing the classical view of phytoplankton cells as only passive drifters, recent research conducted on diverse phytoplankton have shown their ability to sense and respond to changing environmental conditions by employing specific acclimation mechanisms (Falciatore *et al.*, 2000; Vardi *et al.*, 2002, 2006; Montsant *et al.*, 2007; Taylor, 2009; McLachlan *et al.*, 2012; Graff van Creveld *et al.*, 2014).

Viruses have a key role in regulating algal bloom dynamics in addition to other common ecosystem removal pathways such as grazing, nutrient availability and vertical sinking (Bidle, 2015). Viral infection that leads to cell lysis is estimated to turn over at least 20% of the photosynthetic biomass (Brussaard *et al.*, 1995; Agusti *et al.*, 1998; Suttle, 2005; Lehahn *et al.*, 2014). Thus, viruses have a huge impact on ocean biogeochemical cycles by short-circuiting the flux of carbon and nutrients from phytoplankton and bacteria to higher trophic levels, shunting it to the pool of dissolved and particulate organic matter, and making it more available for recycling by microbial respiration (Fuhrman, 1999; Wilhelm and Suttle, 1999; Suttle, 2007). Marine viruses are known to regulate phytoplankton population size, distribution and composition by eliminating more dominant phytoplankton species and are considered major vehicles for horizontal gene transfer between distantly related species (Lindell *et al.*, 2005; Suttle, 2005; Rohwer and Thurber, 2009; Sharon *et al.*, 2009; Winter *et al.*, 2010; Breitbart, 2012).

E. huxleyi is the most abundant and widespread coccolithophore species in the modern oceans (Holligan *et al.*, 1983; Balch *et al.*, 1992; Brown and Yoder, 1994). It forms massive annual spring blooms that are detectable from space by satellites and affects global climate and biogeochemical cycles

Correspondence: A Vardi, Department of Plant and Environmental Sciences, Weizmann Institute of Science, Rehovot 7610001, Israel.
E-mail: assaf.vardi@weizmann.ac.il
Received 26 October 2014; revised 13 October 2014; accepted 6 November 2015; published online 19 January 2016

of carbon and sulfur (Hatton *et al.*, 2004; Rost and Riebesell, 2004; Tyrrell and Merico, 2004). *E. huxleyi* blooms are routinely infected and terminated by specific giant double-stranded DNA coccolithoviruses (*Phycodnaviridae*) (Bratbak *et al.*, 1993; Brussaard *et al.*, 1996; Schroeder *et al.*, 2002; Wilson *et al.*, 2002; Lehahn *et al.*, 2014), the *E. huxleyi* virus (EhV), which is part of the nucleocytoplasmic large DNA virus (*Asfarviridae*, *Ascoviridae*, *Iridoviridae*, *Marseilleviridae*, *Megaviridae*, *Mimiviridae*, *Pandoraviridae*, *Phycodnaviridae*, *Pithoviridae* and *Poxviridae*) clade. EhV encodes for an almost complete *de-novo* biosynthetic pathway for ceramide (Wilson *et al.*, 2005), a sphingolipid known to induce apoptosis in animals and plants (Pettus *et al.*, 2002; Liang *et al.*, 2003). This pathway was recently shown to have a critical role in EhV replication and in induction of *E. huxleyi* programmed cell death in cultures and during natural bloom demise (Pagarete *et al.*, 2009; Vardi *et al.*, 2009, 2012). The viral-induced programmed cell death includes membrane blebbing, induction of caspase-like activity, expression of metacaspases and accumulation of reactive oxygen species (ROS) and specific viral-derived glycosphingolipids (Evans *et al.*, 2006; Bidle *et al.*, 2007; Vardi *et al.*, 2009, 2012). Nonetheless, the cellular signaling and infection mechanisms during the interaction of *E. huxleyi* with its specific virus are poorly understood.

ROS are highly reactive forms of oxygen (radicals and non-radicals), usually regular by-products of oxygen metabolism from photosynthesis, oxidative phosphorylation or peroxisomal activity (Halliwell and Gutteridge, 1986; Asada, 2006; Halliwell, 2006). In high doses, ROS can be very harmful to living cells, ultimately leading to induction of cell death (Van Breusegem and Dat, 2006). In order to avoid the damage caused by ROS, aerobic organisms developed an antioxidant machinery to control the levels of different reactive species. This antioxidant system is composed of ROS-scavenging enzymes and small molecules. Among the ROS-scavenging enzymes are superoxide dismutase, ascorbate peroxidase (APX), catalase (CAT), glutathione (GSH) peroxidase and peroxiredoxin. These enzymes are encoded by the antioxidant gene network and are present in almost all organelles (Apel and Hirt, 2004; Mittler *et al.*, 2004; Halliwell, 2006). Among the small-molecule antioxidants are GSH, ascorbic acid and nicotinamide adenine dinucleotide phosphate (NADPH). These molecules comprise the reductive pool of the cell and react directly with oxidizing agents or through enzymatic reactions mediated by the different antioxidant enzymes listed above (Mittler, 2002). Controlled by the cellular antioxidant system, ROS is a key signaling factor that mediates acclimation responses to environmental stress conditions (Foyer and Noctor, 2003; Mittler *et al.*, 2004; D'Autréaux and Toledano, 2007; Dangoor *et al.*, 2012). Recent reports proposed an important role for ROS metabolism in algal response to environmental stress, such as iron limitation, allelopathy, UV stress, photo-acclimation and oxidative stress (Rijstenbil, 2002; Sukenik *et al.*, 2002; Vardi *et al.*, 2002, 2007; Janknegt *et al.*, 2008; Li *et al.*, 2009; Murik and Kaplan, 2009; Fischer *et al.*, 2012; Thamatrakoln *et al.*, 2012; Graff van Creveld *et al.*, 2014; Murik *et al.*, 2014). As environmental stress conditions can eventually determine the fate of large-scale oceanic blooms, ROS-mediated responses may have an impact on large biogeochemical cycles.

In this study, we investigate the role of ROS metabolism in *E. huxleyi* cells during viral infection. By mapping gene expression data onto antioxidant metabolic pathways, we predicted an increase in GSH biosynthesis, dehydroascorbic acid reduction and H_2O_2 metabolism during lytic infection. Flow cytometry analysis, confocal microscopy and multispectral imaging flow cytometry coupled to biochemical assays showed that H_2O_2 and GSH accumulate in different subcellular localizations only within a subpopulation of infected cells. When the induction of ROS production was inhibited, viral production and cell death were strongly reduced. These findings reveal the importance of ROS and redox metabolism in the viral infection mechanism of *E. huxleyi*.

Materials and methods

Culture growth and viral infection

The non-calcifying *E. huxleyi* strain CCMP2090 was used for this study. Cells were cultured in K/2 medium (Keller *et al.*, 1987) and incubated at 18 °C with a 16:8 h. light–dark illumination cycle. A light intensity of 100 μmol photons $m^{-2}\,s^{-1}$ was provided by cool white light-emitting diode lights. All experiments were performed with exponential phase cultures (5×10^5–1×10^6 cells ml^{-1}). The virus used for this study is EhV86 (Schroeder *et al.*, 2002). In all infection experiments, *E. huxleyi* was infected with 1:50 volumetric ratio of viral lysate to culture (multiplicity of infection of ~1:1 viral particles per cell).

Bioinformatic analysis

A list of candidate genes involved in ROS and antioxidant metabolism was used according to (Mittler *et al.*, 2004). Protein sequences of the target gene from human, *Arabidopsis thaliana*, *Saccharomyces cerevisiae* and, if necessary, additional species were compared with the *E. huxleyi* genome (Read *et al.*, 2013) on the JGI genome website using TBlastN (Altschul *et al.*, 1997). TBlastN hits on the *E. huxleyi* genome were manually defined, aligned and compared with different closely related sequences as previously described by Feldmesser *et al.* (2014). Expression

data for putative genes participating in ROS and antioxidant metabolism was extracted from the database produced by Rosenwasser *et al.* (2014) and presented as the calculated log2 of the expression relative to uninfected control in the same time point.

Peroxidase activity
Peroxidase activity was measured using Amplex Red (Invitrogen, Carlsbad, CA, USA) according to the manufacturer's instructions.

Flow cytometry
Flow cytometry analysis was done on either Eclipse (Sony Biotechnology Inc., Champaign, IL, USA) or LSRII (BD, Franklin Lakes, NJ, USA) flow cytometer, both equipped with 405 and 488 nm solid-state air-cooled lasers, and with standard optic filter set-up. For each sample a minimum of 5000 events were acquired.

Enumeration of cell abundance
Cells were monitored and quantified using an Eclipse (iCyt) flow cytometer. Cells were identified by plotting the chlorophyll fluorescence (663–737 nm) versus green fluorescence (500–550 nm) or side scatter.

Enumeration of viral abundance
For extracellular viral counts, samples were fixed with a final concentration of 0.5% glutaraldehyde for 30 min at 4 °C, then plunged into liquid nitrogen and stored at − 80 °C until analysis. After thawing, samples were stained with SYBR gold (Invitrogen) that was diluted 1:10 000 in Tris–EDTA buffer, incubated for 20 min at 80 °C and cooled to room temperature (RT). Samples were analyzed by an Eclipse flow cytometer (excitation (ex): 488 nm and emission (em): 500–550 nm), minimum of 50 000 events were collected.

Cell death analysis
For cell death analysis, samples were stained with a final concentration of 1 μM Sytox Green (Invitrogen), incubated in the dark for 1 h at RT and analyzed by an Eclipse flow cytometer (ex: 488 nm and em: 500–550 nm). An unstained sample was used as control to eliminate the background signal.

Detection of intracellular ROS
For general ROS analysis, samples were stained with 5 μM CM-H2DCFDA (Invitrogen). Samples were incubated at RT in the dark for 1 h before analysis by an Eclipse flow cytometer (ex: 488 nm and em: 500–550 nm) and compared with an unstained sample. Bes-H_2O_2-AC (Waco, Osaka, Japan) at a final concentration of 50 μM and Bes-SO-AM (Waco) at a final concentration of 30 μM were used for specific detection of H_2O_2 and superoxide, respectively. Samples were incubated with the different stains for 30 min at RT in the dark before being analyzed by an Eclipse flow cytometer (ex: 488 nm and em: 500-550 nm). An unstained sample was used as control to eliminate the background signal.

Total GSH, GSH, GSSG and GSH/GSSG ratio
GSH was measured by the recycling assay, GSH reductase-dependent reduction of 5,5′-dithiobis(2-nitro-benzoic acid) (Ellman's reagent; Tietze, 1969) adjusted for microplate assay (Queval and Noctor, 2007). Briefly, 400 ml cultures were pelleted by mean of centrifugation (17 000 *g*, 10 min, 4 °C) plunged in to liquid nitrogen and were kept in − 80 °C. Extractions were performed in 1 M $HClO_4$ to minimize GSH oxidation. On adjustment of pH to 6 by phosphate buffer and KCO_3, part of the extract was reacted with 2-vinylpyridine for quantification of oxidized GSH (GSSG). Both (total and GSSG) were quantified by a standard curve of known concentrations of GSH and GSSG for the reaction kinetics. Quantities of total GSH, GSSG and GSH were calculated from concentration and volumes, and normalized to cell abundance at time of collection.

Detection of intracellular GSH
Monochlorobimane (mBCl, Sigma-Aldrich, Rehovot, Israel) was added to the samples to a final concentration of 50 μM and incubated for 30 min at RT in the dark, then detected using an Eclipse flow cytometer (ex: 405 nm and em: 430–480 nm). An unstained sample was used as control to eliminate the background signal.

Co-staining for GSH and H_2O_2
mBCl and Bes-H_2O_2 (50 and 30 μM, respectively) were applied to the cells simultaneously. For each treatment, an unstained sample and a single stain for each dye was assessed by the same method. All samples were analyzed by an LSRII flow cytometer (BD) using the blue (ex: 405 nm and em: 430–480 nm) and green (ex: 488 nm and em: 500–550 nm) channels. Stained samples were also observed by confocal microscopy using a Nikon Eclipse Ti-E microscope (Tokyo, Japan) with Nikon A1+ confocal laser system equipped with CFI PLAN APO VC × 60A WI and CFI Plan Apochromatic × 100 Lambda objectives. For mBCl excitation a 405 nm 100 mW laser was used with 470 nm emission collection filter, for Bes-H2O2 excitation a Sapphire 488 nm 50 mW laser was used with 525 nm emission collection filter and for chlorophyll excitation a 640 nm 100 mW laser was used with 700 nm emission collection filter. Acquired images were analyzed using NIS-Elements AR imaging software. For multispectral imaging flow cytometry, cells were stained as described and 5000 cells were collected from each sample using ImageStreamX

flow cytometer (Amnis Corp., Seattle, WA, USA; Millipore, Darmstadt, Germany). Data were analyzed using image analysis software (IDEAS 6.0; Amnis Corp., Millipore). Images were compensated for fluorescent dye overlap by using single-stain yeast cells as non-chlorophyll-containing controls. Cells were gated for single cells using the area and aspect ratio features, and for focused cells using the Gradient RMS feature, as previously described (George *et al.*, 2006). Cells were gated for positive signal of chlorophyll, mBCl and Bes-H_2O_2 (for GSH and H_2O_2, respectively). The co-localization for the two dyes was quantified using the bright detail similarity feature (the log base 2 transformed Pearson's correlation coefficient of the localized bright spots in the two input images; George *et al.*, 2006).

Cell sorting
Cells were sorted according to their mBCl and Bes-H_2O_2 signals using SORP FACSAriaII cell sorter (BD) equipped with 405 and 488 nm solid-state air-cooled lasers, and with standard optic filter set-up. About one million cells were sorted in purity mode from each stained population. Cells were collected on GF/F filters, plunged in liquid nitrogen and stored in −80 °C before quantitative PCR analysis for viral abundance.

Enumeration of intracellular viral abundance
For intracellular viral DNA quantification, DNA was extracted from GF/F filters as previously described (Schroeder *et al.*, 2002) and then used for quantitative PCR analysis with the major capsid protein primers (Pagarete *et al.*, 2009). All reactions were performed in four biological replicates and technical duplicates. For all reactions, Platinum SYBER Green qPCR SuperMix-UDG with ROX (Invitrogen) was used as described by the manufacturer. Reactions were performed on StepOnePlus real-time PCR systems (Applied Biosystems, Foster City, CA, USA) as follows: 50 °C for 2 min, 95 °C for 2 min, 40 cycles of 95 °C for 15 s and 60 °C for 30 s. Results were calibrated against serial dilutions of EhV201 DNA at known concentrations, enabling exact enumeration of viral abundance, and normalized to cell numbers collected on filters.

Detection of carbonylated proteins
OxyBlot Protein Oxidation Detection Kit (Millipore, Darmstadt, Germany) was used according to the manufacturer's instructions for the assessment of cellular oxidative damage.

Application of peroxidase inhibitor and ROS scavenger
Esculetin, an inhibitor of peroxidase activity (Dunand *et al.*, 2007; Zhang *et al.*, 2008), was dissolved in dimethyl sulfoxide and applied to cultures to a final concentration of 50 μM, 1 h before infection. Potassium iodide, an H_2O_2 scavenger (Dunand *et al.*, 2007), was dissolved in distilled water and added to cultures to a final concentration of 1 mM, 1 h before infection and on every consecutive day.

Statistical analysis
All reported *P*-values were determined using a two-tailed unpaired Student's *t*-test and presented in figures were $*P<0.1$, $**P<0.05$ and $***P<0.01$. In all figures, error bars represent s.e. and '*n*' defined as the number of unrelated replicas of each treatment.

Results

Expression profile of ROS metabolism genes during EhV infection
To explore the role of ROS during viral infection, we examined the expression profile of selected genes that participate in cellular ROS metabolism (Mittler *et al.*, 2004). Complete DNA sequences of the target genes were manually defined based on genomic sequences, expressed sequence tags and RNA sequencing data as described in the Materials and Methods section. Expression data for each of the defined genes was generated based on RNA sequencing transcriptome analysis of RNA derived from *E. huxleyi* cells at 1 and 24 h post infection (hpi) with the lytic virus EhV201 or the non-lytic virus EhV163, and normalized to expression levels in uninfected cells at the same time point (Feldmesser *et al.*, 2014; Rosenwasser *et al.*, 2014). Changes were observed in expression levels of several transcripts involved in the biosynthesis and recycling of GSH and ascorbate, important low-molecular-weight antioxidants (Foyer and Noctor, 2005). Genes that encode for glutamate cysteine ligase and GSH synthase, key enzymes in the GSH biosynthesis pathway, were increased 2.4-fold at 24 hpi (Figure 1). The expression of GSH reductase transcript increased 1.4-fold at 24 hpi (Figure 1). The ascorbate recycling enzyme dehydroascorbate reductase had no homolog in the *E. huxleyi* genome. GSH *S*-transferase omega (*GSTO*) gene, which exhibited dehydroascorbate reductase activity in human and other animal systems (Board *et al.*, 2000), increased its expression levels by 1.7-fold at 24 hpi. Although genes involved in production or recycling of ascorbate and GSH were generally upregulated, the expression level of *APX*, an enzyme that depends on ascorbate as an electron donor, increased up to 1.4-fold at 1 hpi but was three times lower than uninfected control at 24 hpi (Figure 1). On the other hand, transcript levels of the GSH peroxidase enzyme that uses GSH as a reducing agent increased by 1.7-fold at 1 hpi and 1.3-fold at 24 hpi (Figure 1).

Expression levels of NADPH oxidase, a producer of superoxide, increased by 4.1-fold at 24 hpi, whereas superoxide dismutase and *CAT* expression, both antioxidant enzymes that scavenge superoxide

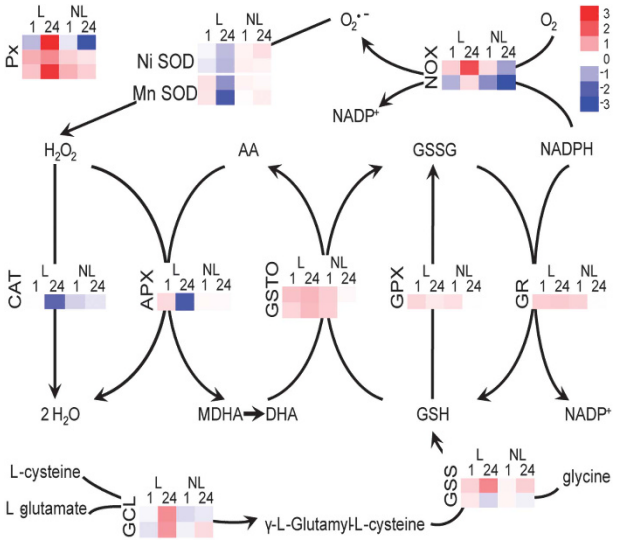

Figure 1 Gene expression profiles of ROS and redox-related transcripts during *E. huxleyi* viral infection. *E. huxleyi* infected with the lytic (L) virus EhV201 or with the non-lytic (NL) virus EhV163. Red, upregulation; blue, downregulation; scale values refer to log base 2 of reads per milion (RPM) normalized to uninfected control at the same time point. AA, ascorbic acid; *APX*, ascorbate peroxidase; *CAT*, catalase; DHA, dihydroascorbate; *GCL*, glutamate cysteine ligase; *GPX*, GSH peroxidase; *GR*, GSH reductase; GSH, glutathione; *GSS*, GSH synthase; GSSG, oxidized GSH; *GSTO*, GSH *S*-transferase omega; MDHA, monodihydroascorbate; NADPH-nicotinamide adenine dinucleotide phosphate; *NOX*, NADPH oxidase; *Px*, peroxidase; *SOD*, superoxide dismutase.

and H_2O_2, respectively, were 3.2- and 2.5-fold lower then uninfected control, respectively, at 24 hpi (Figure 1). The most dominant elevation in expression, up to 7-fold at 24 hpi, was found for transcripts encoded by gene homologs of peroxidases (Figure 1). Some of these genes are known to produce ROS as H_2O_2 or superoxide radical, whereas other functions attributed to this gene family are antioxidant activity and specifically the catalysis of H_2O_2 degradation. Only minor changes in expression of these genes were found in *E. huxleyi* cultures treated with the non-lytic virus EhV163, with the exception of NADPH oxidase and peroxidase transcript levels that decreased in expression. Taken together, our data reveal a major remodeling in expression of transcripts related to ROS metabolism that occurs in *E. huxleyi* cells as a result of viral infection.

Viral infection is associated with host co-generation of H_2O_2 and GSH

The simultaneous rise in ROS and GSH levels during infection was associated with induction of host cell death and viral production. A decline in host cell abundance was observed from 72 hpi onwards (Figure 2a), together with accumulation of EhV in the culture media (Figure 2b), and rapid increase of cell death detected using Sytox Green as a proxy for compromised membrane integrity (Figure 2c). The onset of the lytic phase of infection (72 hpi) was characterized by significant induction in ROS accumulation as detected by CM-H_2DCF DA (Figure 2d, Student's *t*-test, *P*-value = 0.01). In order to assess whether specificity in ROS chemical species have a role in onset of lytic infection, we used specific ROS stains to either superoxide (detected by Bes-SO) or H_2O_2 (detected by Bes-H_2O_2). Where superoxide levels varied only slightly (Figure 2e), levels of H_2O_2 exhibited a profound increase during lytic phase of viral infection (Figure 2f). In order to examine the impact of oxidative stress on protein oxidation, we analyzed carbonylated proteins detected by OxyBlot during infection. This analysis showed accumulation of oxidized proteins in infected cells already at early stages (>4 hpi), whereas uninfected cells started accumulating damaged proteins only at later stages of growth (Supplementary Figure S1).

The fluorescent stain mBCl was further used to complement ROS measurement with quantification of intracellular GSH levels. Although GSH levels in uninfected control cells decreased slightly as the culture aged, GSH accumulated in infected cells beginning at 48 hpi (Figure 3a). The induction in GSH and H_2O_2 levels accompanied the onset of the lytic phase of infection. In order to compliment the *in vivo* fluorescent-based assay, we employed a biochemical approach to quantify the various GSH pools in the cells during viral infection. Using this biochemical assay, which is based on the GSH reductase-dependent reduction of 5,5′-dithiobis(2-nitro-benzoic acid) (Ellman's reagent; Tietze, 1969; Queval and Noctor, 2007) (Figures 3b–e), we detected an increase in total GSH (GSH+GSSG, Figure 3b) in cell extracts derived from lytic phase of infection. This result was supported by previous research detecting total GSH increase during infection by means of high-performance liquid chromatography (Gledhill *et al.*, 2012). In agreement with the *in vivo* GSH assessment using mBCl fluorescence stain (Figure 3a), at 72 hpi levels of GSH were significantly higher in infected cells in comparison with uninfected cells (Figure 3c, Student's *t*-test, *P*-value = 0.02). Furthermore, large increase in GSSG was detected during viral infection (Figure 3d). These changes in the relative pools of GSH were reflected in a marked decline in the GSH/GSSG ratio (Figure 3e), a ratio that is considered as proxy for the oxidative stress (Noctor and Foyer, 1998; Kranner *et al.*, 2006). Alterations in GSH/GSSG as a result of ROS production can regulate the activation of many biological processes, such as transcription, posttranslational modification and protein–protein interactions, by affecting the oxidation state of thiol groups. Taken together, the profound ROS generation during viral infection had a major consequence on cellular redox metabolism and antioxidant networks as determined by the GSH pools. The gene expression analysis reflected this remodeling where GSH biosynthetic pathways were found to divert towards production and recycling, while genes responsible for H_2O_2 degradation (CAT and APX) decreased in expression level (Figure 1).

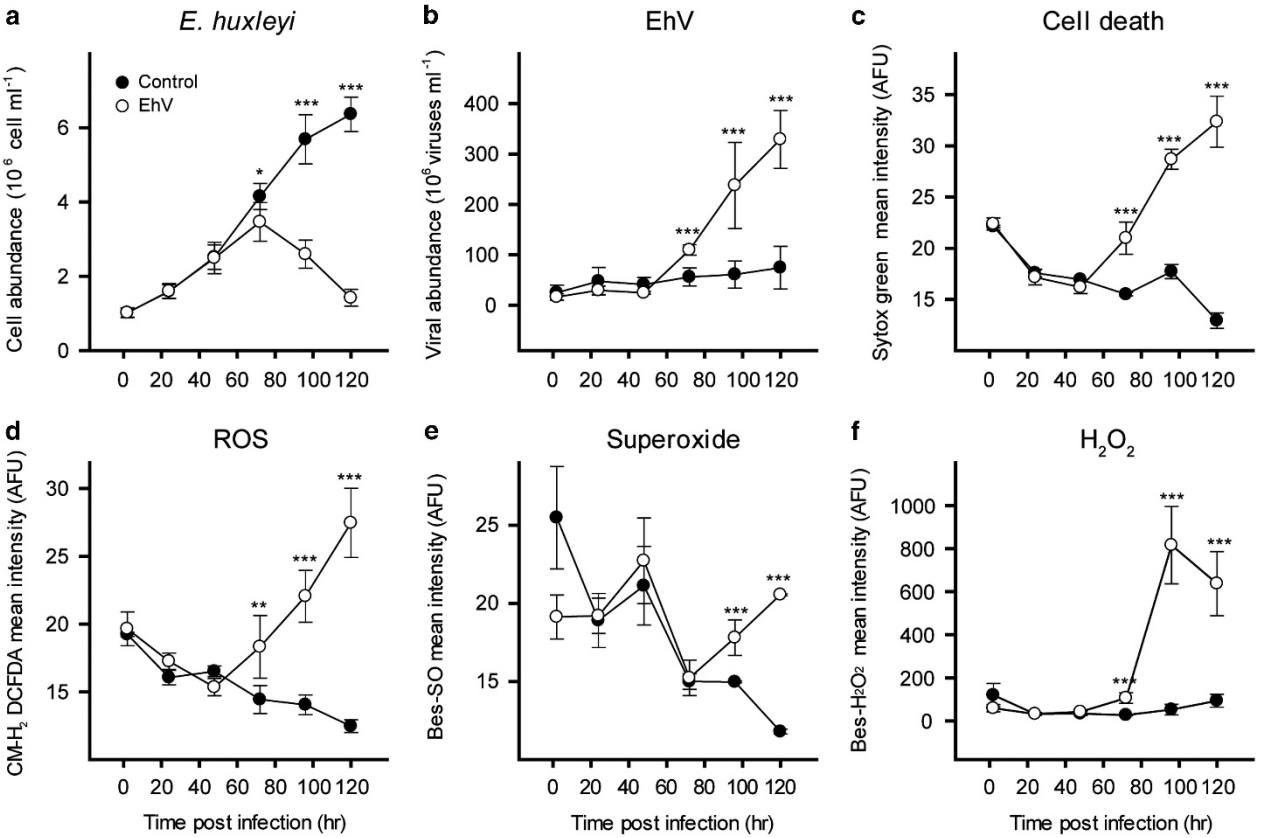

Figure 2 H_2O_2 is the predominant ROS produced during viral infection of *E. huxleyi*. Cell abundance (**a**), extracellular viral abundance (**b**), cell death assessed by Sytox staining (**c**), ROS assesed by CM-H2DCFDA staining (**d**), superoxide measured by Bes-SO staining (**e**) and H_2O_2 measured by Bes-H_2O_2 staining (**f**) of *E. huxleyi* cells infected with lytic virus (empty circles) and uninfected control (full circles). Each data point was calculated based on average flow cytometry fluorescence or count measurements of at least 5000 events per sample point and presented as mean ± s.e., $n=3$. *P*-values were determined using two-tailed unpaired Student's *t*- test ($^*P<0.1$, $^{**}P<0.05$ and $^{***}P<0.01$).

H_2O_2 and GSH accumulate simultaneously in different subcellular localizations of infected cells

The accumulation of GSH (Figure 3a) simultaneously with H_2O_2 production (Figure 2f) raise questions regarding its origin and cellular localization of pro- and antioxidants in infected cells. Flow cytometry analysis of cells co-stained for both H_2O_2 and GSH revealed that the elevation in H_2O_2 occurred in the same subpopulation with increased GSH content (Figure 4). Although in the first day of infection no differences were found between infected cells and control, at 72 hpi 38% of the infected cells were found positive for both H_2O_2 and GSH, as compared with 7% of control cells (Figure 4a). In order to get direct evidence that the dual-stained cells were indeed infected, we sorted GSH- and H_2O_2-positive cells from culture infected for 72 hpi. These cells were subjected to quantitative PCR analysis of viral DNA using major capsid protein primers. This dual-stained subpopulation had fourfold higher viral DNA copy number per cell as compared with cells sorted from GSH- and H_2O_2-negative subpopulation (Figure 4b).

Using confocal microscopy, we subsequently examined the subcellular localization of GSH and H_2O_2 in infected cells. The GSH signal was punctuated in both control and infected cells, while a strong H_2O_2 signal extended only to a vast fraction of infected cells (Figures 5a and b). Interestingly, the two fluorescent signals had different localization within the infected cells and both were excluded from the chloroplast (Figures 5a and b). We further used a multispectral imaging flow cytometry, in order to quantify this observation in a high-throughput manner (>5000 infected *E. huxleyi* cells). In order to estimate the co-localization of the blue (GSH) and green (H_2O_2) signals, the bright detail similarity feature was used as described in the Materials and Methods section. Representative cells with high signal for both H_2O_2 and GSH were chosen for their median similarity score (Figure 5c). In order to calibrate the bright detail similarity value as a co-localization score between GSH and H_2O_2, the same procedure was applied to cells stained with two different DNA stains (Hoechst and Syto13). In comparison with the high-value DNA-stained cells score for their co-localization in the nucleus (population median of 2.0; Figure 5d, blue histogram), infected *E. huxleyi* cells with elevated GSH and H_2O_2 signals showed very low, bright detail

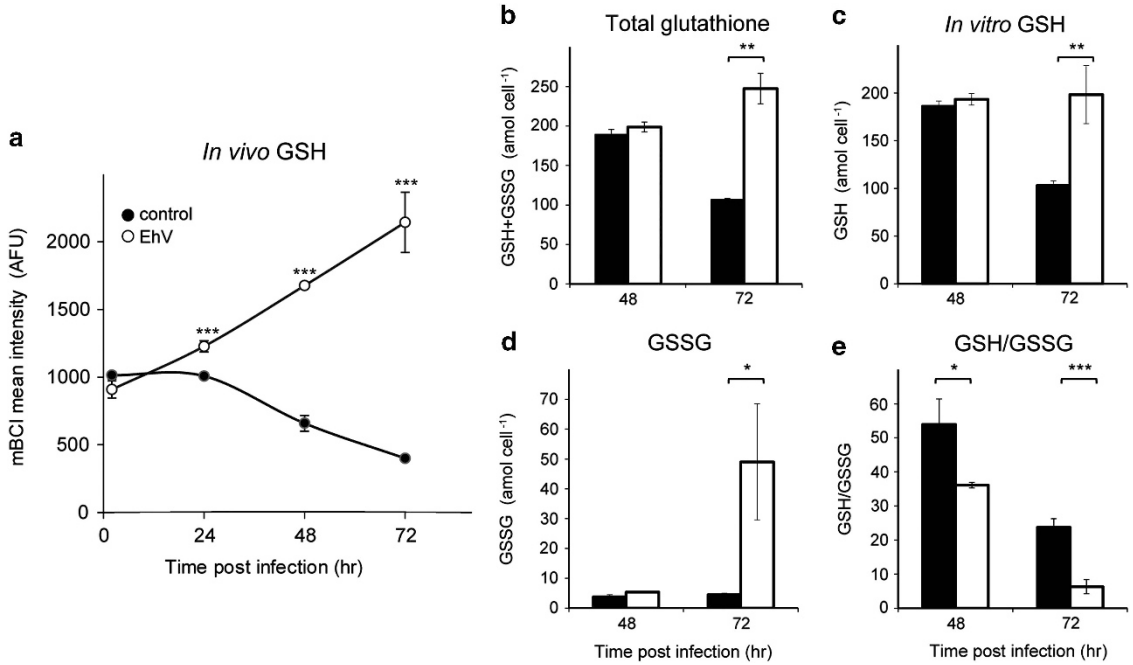

Figure 3 Quantification of total, reduced (GSH) and oxidized (GSSG) pools of GSH, during *E. huxleyi* viral infection. *E. huxleyi* cells infected with lytic virus (empty circles or bars) or uninfected control (full circle or bars) stained by mBCl for quantification of level of reduced GSH (**a**). Each data point was calculated based on average flow cytometry fluorescence measurements of at least 5000 events per sample point and presented as mean ± s.e., $n=3$. Biochemical-based quantification of GSH total (GSH+GSSG), reduced (GSH) and oxidized (GSSG) GSH per cell and GSH/GSSG ratio (**b–e**) in cell extract from control or infected cells, presented as mean ± s.e., $n=4$. *P*-values were determined using two-tailed unpaired Student's *t*-test (*$P<0.1$, **$P<0.05$ and ***$P<0.01$).

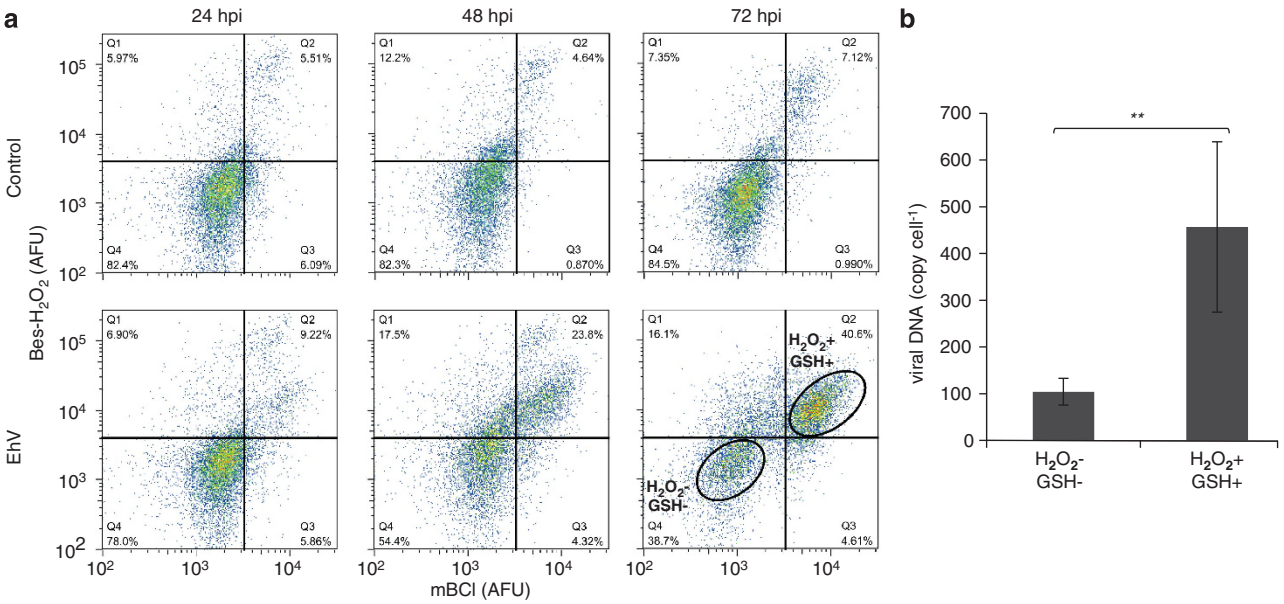

Figure 4 H_2O_2 and GSH co-generated in viral-infected cells. Flow cytometry dot plots showing population dynamics during the course of viral infection. Cells were stained for GSH (mBCl) and H_2O_2 (Bes-H_2O_2). Representative data from at least five experiments are shown (**a**). AFU, arbitrary fluorescent units. Bars showing major capsid protein (MCP) copy number per cell obtained by quantitative PCR (qPCR) analysis for the different GSH and H_2O_2 population sorted (indicated by arrows) out of the two gated population (GSH− H_2O_2− and GSH+ H_2O_2+) at 72 hpi with EhV 86 (**b**), presented as mean ± s.e., $n=4$. *P*-values were determined using two-tailed unpaired Student's *t*-test (**$P<0.05$).

similarity (population median of 0.8; Figure 5d, red histogram). The low score measured for the signals is indicating low co-localization between the two molecules in the cell.

Elevated ROS levels are essential for a successful viral replication cycle

To corroborate the high expression level of peroxidase genes with enzyme activity, we measured

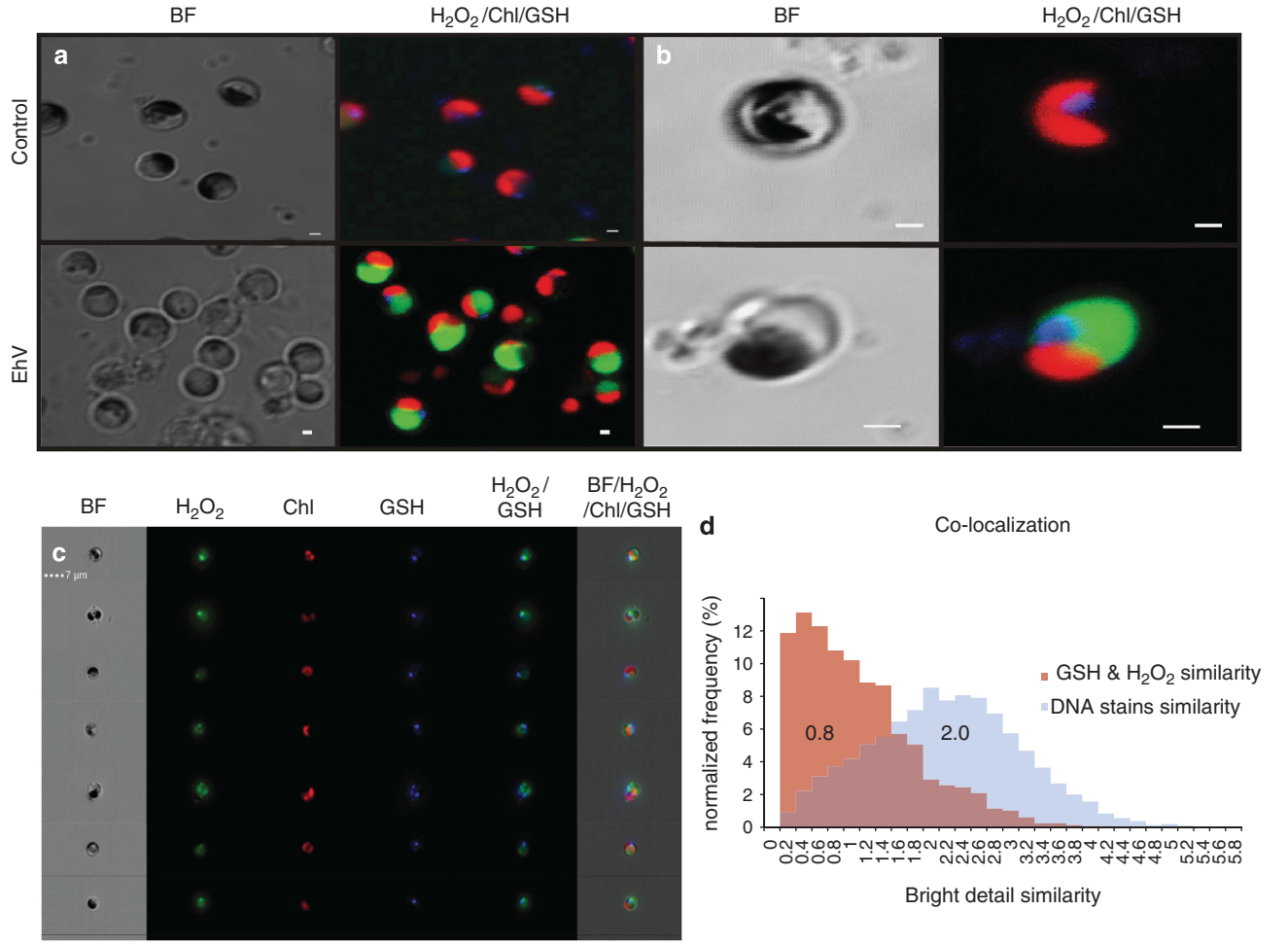

Figure 5 Subcellular localization of GSH and H_2O_2 in infected *E. huxleyi* cells. Confocal fluorescence micrographs detecting subcellular H_2O_2 (Bes-H_2O_2, green fluorescence), GSH (mBCl, blue fluorescence), chlorophyll (red fluorescence) and DIC images of the same fields, in uninfected control (upper panels) or EhV-infected *E. huxleyi* cells (lower panels). Scale bars represent 1 µm (**a**). (**b**) The same samples as in **a** shown in higher magnification; scale bars represent 1 µm. Imaging flow cytometry (Image Stream X) micrographs of representative cells selected for their median bright detail similarity score (0.8), channels of bright field (BF), green (H_2O_2), red (chlorophyll, Chl) and blue (GSH) are presented; scale bar represent 7 µm (**c**). Population distribution of 5000 cells selected for their bright detail similarity between the green and blue fluorescence channels representing spatial co-localization between H_2O_2 and GSH in the cells (red histogram). As positive control for co-localization bright detail similarity score of cells stained with both Syto13 (green DNA stain) and Hoechst (blue DNA stain) are presented (blue histogram) (**d**).

peroxidase activity during infection and found it to increase in the infected culture 2.4-fold above the levels measured in uninfected control (Supplementary Figure S2). Consequently, we used esculetin, a known inhibitor of peroxidase activity, in order to examine the functional role of ROS in the *E. huxleyi*–EhV (Sirois and Miller, 1972; Dunand *et al.*, 2007; Potapovich *et al.*, 2012). Esculetin treatment completely abolished both viral-induced cell death (Figure 6a) and viral production (Figure 6b). Interestingly, esculetin was highly efficient in suppressing H_2O_2 generation and in preventing GSH accumulation (Figures 6c and d). Importantly, suppression of viral release was not due to cytotoxicity of esculetin, as treatment of an uninfected culture with the substance had only a minor effect on cell growth, while esculetin treatment in infected cells showed the same growth as uninfected control (Figure 6a). Furthermore, a similar trend was found in treatment of infected cells with potassium iodide, an H_2O_2 scavenger, significantly decreasing cell death and viral productivity (Supplementary Figures S3a and b, Student's *t*-test, see figure for *P*-values). Taken together, our data strongly support the pivotal role of ROS metabolism orchestrated by a complex stoichiometry between ROS generation and antioxidant regulation during the lytic phase of EhV infection.

Discussion

In this study, we explored the role of ROS metabolism during host–virus interaction of the bloom-forming coccolithophore *E. huxleyi*. ROS was previously proposed to be associated with viral

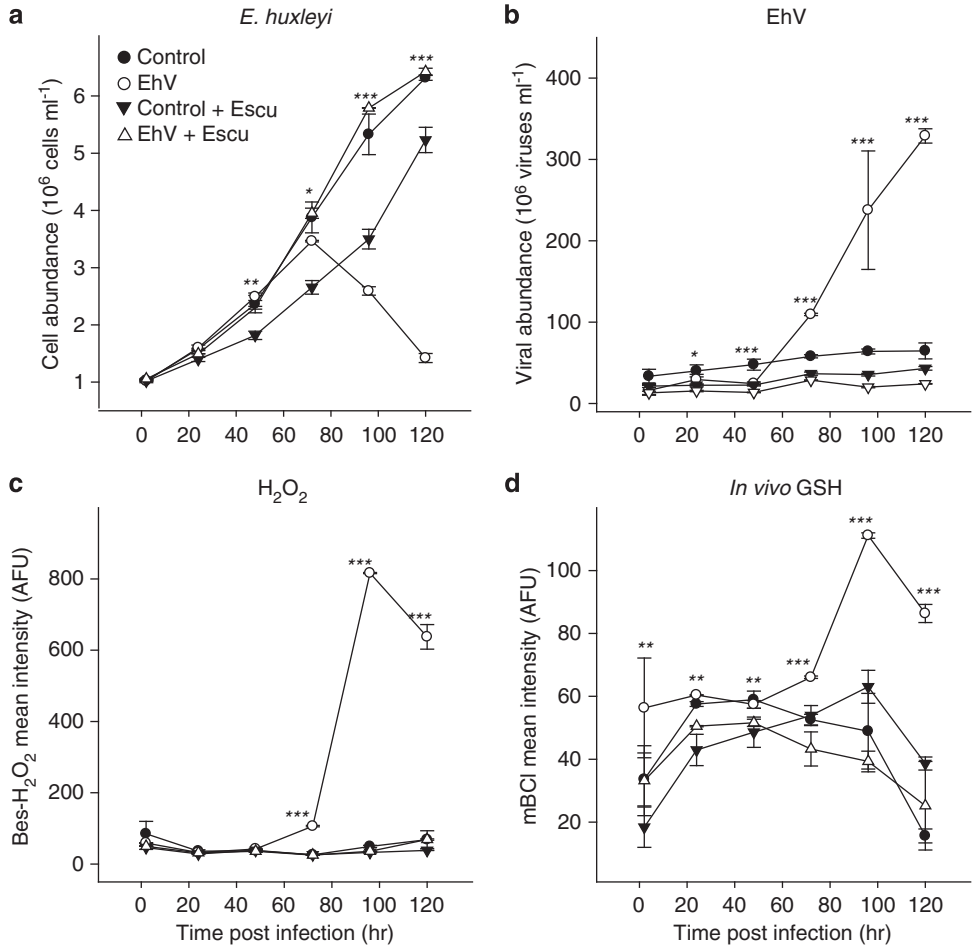

Figure 6 Inhibition of peroxidase activity reduced cell death, viral production, H_2O_2 and GSH accumulation. *E. huxleyi* cell abundance (**a**), EhV viral abundance (**b**), cellular H_2O_2 (**c**) and GSH (**d**) of cultures infected with the lytic virus (empty symbols) and uninfected control (full symbols) treated with 50 μM esculetin (tringles) or untreated cells (circles). Each data point was calculated based on average flow cytometry fluorescence or count measurements of at least 5000 events per sample point and presented as mean ± s.e., $n=3$. *P*-values were determined using two-tailed unpaired Student's *t*-test (*$P<0.1$, **$P<0.05$ and ***$P<0.01$) calculated in each time point between esculetin-treated and -untreated infected *E. huxleyi* cultures.

infection and specifically with induction of hallmarks of programmed cell death during the lytic phase of infection in *E. huxleyi* cultures (Evans *et al.*, 2006) and mesocosm experiments (Vardi *et al.*, 2012). Recent reports have shown a reduction in the photosystem II efficiency, chlorophyll degradation and carotenoid production during *E. huxleyi* infection, supporting a possible source for ROS generation (Evans *et al.*, 2006; Bidle *et al.*, 2007; Llewellyn *et al.*, 2007; Bale *et al.*, 2013; Kimmance *et al.*, 2014). Our transcriptome analysis suggested an additional enzymatic source for ROS production by induction of NADPH oxidase (Figure 1). Reduction in APX and CAT expression implied a compromised antioxidant capacity and H_2O_2 accumulation that may mediate viral-induced cell death during lytic phase of viral infection (Figure 1).

As diverse environmental stress conditions trigger ROS, one of the key questions is how specificity in ROS signaling is being achieved in order to regulate cell fate in marine phytoplankton. Our data demonstrated that H_2O_2, and not superoxide, is the dominant intracellular ROS that accumulates during the onset of the lytic phase of viral infection (Figures 2e and f). The interplay between H_2O_2 and superoxide was found to be an essential factor in determining cell fate in different model systems (Bloomfield and Pears, 2003; Lardy *et al.*, 2005; Owusu-Ansah and Banerjee, 2009; Tsukagoshi *et al.*, 2010). The transcriptomic analysis presented here suggested that viral infection triggered H_2O_2 production, presumably by activation of a combination of NADPH oxidase and/or specific peroxidases, while decreasing the degradation of H_2O_2 by down-regulating CAT and APX (Figure 1). Such changes in expression patterns can enable transduction of specific ROS signaling cascades that might orchestrate the final stage of viral infection and cell lysis (Veal *et al.*, 2007; Go and Jones, 2008; Shao *et al.*, 2008; Mittler *et al.*, 2011; Siddique *et al.*, 2014).

ROS has an important role in facilitating different stages of viral infection cycle in diverse virus host systems such as Kaposi's sarcoma-associated herpes

virus, hepatitis C virus and HIV (Perl and Banki, 2000; Ye *et al*., 2011; Bottero *et al*., 2013; Ma *et al*., 2013). On the other hand, in plants, during tobacco mosaic virus infection, ROS signaling was found to initiate plant defense hypersensitive response (Allan *et al*., 2001; Yoda *et al*., 2003; Love *et al*., 2005). Interestingly, chlorella virus, a close relative of EhV within the nucleo-cytoplasmic large DNA virus family, was found to encode a superoxide dismutase protein (Kang *et al*., 2014). Our data show that ROS, and specifically H_2O_2, is a crucial factor during EhV infection, whereby inhibition of peroxidase activity using esculetin or scavenging of H_2O_2 using potassium iodide resulted in a reduction in host cell death and a decline in viral production (Figures 6a and b, and Supplementary Figures S3a and b). These results add a new angle to the role of ROS as a key factor in the EhV viral replication cycle.

Typically, a rise in ROS production during stress occurs concomitant with a decrease in the antioxidant capacity (Foyer and Noctor, 2011). In contrast, we report that the rise in ROS concentration was accompanied by maintaining high GSH quota and a rise in GSSG and total GSH during the late stage of viral infection under a highly oxidizing cellular environment (Figures 3–5). These data may reflect the observed pattern of gene expression in the infected host's transcriptome driving the GSH-ascorbate cycles. The essential pathways that maintain the reducing pools of GSH and ascorbate, such as GSH biosynthesis genes (*GCL* and *GSS*), as well as GSH and ascorbate recycling genes (*GR* and *GSTO*), were upregulated during infection (Figure 1). The observed overproduction of total GSH in parallel to decline in the GSH/GSSG ratio may point to increase in the flux through the GSH biosynthesis and GSH/ascorbate pathways. These changes might serve the purpose of maintaining a high ratio of reduced to oxidized ascorbate, which was reported to precondition the cell sensitivity to oxidative stress, regulating cell death (Murik and Kaplan, 2009; Murik *et al*., 2014). Similarly, keeping a high cellular GSH concentration can serve an important function in maintaining host metabolism and newly synthesized viral proteins under the highly oxidative microenvironment of the infected cell. It was recently shown that a decrease in cellular GSH concentrations can serve as an early event in the apoptotic cascade, and that low antioxidant capacity can lead to initiation of a programmed death cascade (Circu and Aw, 2008; Franco and Cidlowski, 2009). Thus, viral replication might benefit from high intracellular GSH content (Gledhill *et al*., 2012), prolonging cell viability and circumventing premature cell death that might be induced as a defense strategy of the host.

Furthermore, EhV replication has a high demand for nucleotides to support the synthesis and replication of its large genome (Wilson *et al*., 2005) and high burst size (Bratbak *et al*., 1993). This metabolic demand can be fulfilled by converting ribonucleotides to deoxy ribonucleotides via ribonucleotide-diphosphate reductase activity, which in turn has to be reduced by thioredoxin or by glutaredoxin, in the second drawing the reducing power out of the GSH pool (Gon *et al*., 2006). This possibility underlines the importance of the increase in GSH metabolism during infection, while also suggesting why this virus harbors an *RNR* gene in its genome (Wilson *et al*., 2005).

ROS metabolism was recently shown to be an important feature of algal response to environmental stress by mediating important cellular responses, which eventually determine the fate of cells. ROS take part in the response of diatoms to iron limitation (Thamatrakoln *et al*., 2012), in dinoflagellate response to CO_2 limitation and to mediate allelopathic interactions with toxic cyanobacteria (Vardi *et al*., 1999; Sukenik *et al*., 2002; Vardi *et al*., 2002), in response to UV radiation and photoacclimation (Rijstenbil, 2002; Janknegt *et al*., 2008; Li *et al*., 2009; Fischer *et al*., 2012), and as a secondary burst during oxidative stress and senescence (Vardi *et al*., 2007; Murik and Kaplan, 2009; Murik *et al*., 2014). We suggest that during the host–virus interactions, EhV subverts the cellular antioxidant and ROS metabolism for its benefit, to ensure an optimal replication cycle. Taken together, the results presented here clearly imply a pivotal role for ROS metabolism during this host–virus interaction. ROS can mediate the cross-talk between the main cellular pathways that are triggered during EhV infection: autophagy (Schatz *et al*., 2014), sphingolipid metabolism (Vardi *et al*., 2009) and programmed cell death (Bidle *et al*., 2007), and therefore will determine the fate of the viral-infected blooms and influence the cycling of nutrients and carbon within microbial food webs in the marine ecosystem. We propose using this unique set of cellular markers as a novel tool to assess viral infection at different phases of algal blooms in the ocean.

Conflict of Interest

The authors declare no conflict of interest.

Acknowledgements

We thank Daniella Schatz for fruitful discussions and commenting on the manuscript. We thank Ester Feldmesser for assistance with data analysis. This research was supported by the European Research Council (ERC) StG (INFOTROPHIC grant number 280991), the Israeli Science Foundation (ISF) Legacy Heritage fund (grant number 1716/09) and the generous support of Edith and Nathan Goldenberg Career Development Chair both awarded to AV.

References

Agusti S, Satta MP, Mura MP, Benavent E. (1998). Dissolved esterase activity as a tracer of phytoplankton lysis: evidence of high phytoplankton lysis rates in the northwestern Mediterranean. *Limnol Oceanogr* **43**: 1836–1849.

Allan AC, Lapidot M, Culver JN, Fluhr R. (2001). An early tobacco mosaic virus-induced oxidative burst in

tobacco indicates extracellular perception of the virus coat protein. *Plant Physiol* **126**: 97–108.
Altschul SF, Madden TL, Schäffer AA, Zhang J, Zhang Z, Miller W *et al.* (1997). Gapped BLAST and PSI-BLAST: a new generation of protein database search programs. *Nucleic Acids Res* **25**: 3389–3402.
Apel K, Hirt H. (2004). Reactive oxygen species: metabolism, oxidative stress, and signal transduction. *Annu Rev Plant Biol* **55**: 373–399.
Asada K. (2006). Production and scavenging of reactive oxygen species in chloroplasts and their functions. *Plant Physiol* **141**: 391–396.
Balch WM, Holligan PM, Kilpatrick KA. (1992). Calcification, photosynthesis and growth of the bloom-forming coccolithophore *Emiliania huxleyi*. *Cont Shelf Res* **12**: 1353–1374.
Bale NJ, Airs RL, Kimmance SA, Llewellyn CA. (2013). Transformation of chlorophyll a during viral infection of *Emiliania huxleyi*. *Aquat Microb Ecol* **69**: 205–210.
Behrenfeld MJ, O'Malley RT, Siegel DA, McClain CR, Sarmiento JL, Feldman GC *et al.* (2006). Climate-driven trends in contemporary ocean productivity. *Nature* **444**: 752–755.
Bidle KD, Haramaty L, Barcelos E, Ramos J, Falkowski P. (2007). Viral activation and recruitment of metacaspases in the unicellular coccolithophore *Emiliania huxleyi*. *Proc Natl Acad Sci USA* **104**: 6049–6054.
Bidle KD. (2015). The molecular ecophysiology of programmed cell death in marine phytoplankton. *Ann Rev Mar Sci* **7**: 341–375.
Bloomfield G, Pears C. (2003). Superoxide signalling required for multicellular development of *Dictyostelium*. *J Cell Sci* **116**: 3387–3397.
Board PG, Coggan M, Chelvanayagam G, Easteal S, Jermiin LS, Schulte GK *et al.* (2000). Identification, characterization, and crystal structure of the Omega class glutathione transferases. *J Biol Chem* **275**: 24798–24806.
Bottero V, Chakraborty S, Chandran B. (2013). Reactive oxygen species are induced by Kaposi's sarcoma-associated herpesvirus early during primary infection of endothelial cells to promote virus entry. *J Virol* **87**: 1733–1749.
Bratbak G, Egge JK, Heldal M. (1993). Viral mortality of the marine alga *Emiliania huxleyi* (Haptophyceae) and termination of algal blooms. *Mar Ecol Prog Ser* **93**: 39–48.
Breitbart M. (2012). Marine viruses: truth or dare. *Ann Rev Mar Sci* **4**: 425–448.
Brown CW, Yoder JA. (1994). Coccolithophorid blooms in the global ocean. *J Geophys Res Ocean* **99**: 7467–7482.
Brussaard CPD, Kempers RS, Kop AJ, Riegman R, Heldal M. (1996). Virus-like particles in a summer bloom of Emiliania huxleyi in the North Sea. *Aquat Microb Ecol* **10**: 105–113.
Brussaard CPD, Riegman R, Noordeloos AA, Cadee GC, Witte H, Kop AJ *et al.* (1995). Effects of grazing, sedimentation and pyhtoplankton cell lysis on the structure of a coastal pelagic food web. *Mar Ecol Prog Ser* **123**: 259–271.
Circu ML, Aw TY. (2008). Glutathione and apoptosis. *Free Radic Res* **42**: 689–706.
Dangoor I, Peled-Zehavi H, Wittenberg G, Danon A. (2012). A chloroplast light-regulated oxidative sensor for moderate light intensity in *Arabidopsis*. *Plant Cell* **24**: 1894–1906.
Dunand C, Crevecoeur M, Penel C, Crèvecoeur M. (2007). Distribution of superoxide and hydrogen peroxide in *Arabidopsis* root and their influence on root development: possible interaction with peroxidases. *New Phytol* **174**: 332–341.
D'Autréaux B, Toledano MB. (2007). ROS as signalling molecules: mechanisms that generate specificity in ROS homeostasis. *Nat Rev Mol Cell Biol* **8**: 813–824.
Evans C, Malin G, Mills GP, Wilson WH. (2006). Viral infection of *Emiliania Huxleyi* (Prymnesiophyceae) leads to elevated production of reactive oxygen species. *J Phycol* **42**: 1040–1047.
Falciatore A, D'Alcala MR, Croot P, Bowler C. (2000). Perception of environmental signals by a marine diatom. *Science* **288**: 2363–2366.
Feldmesser E, Rosenwasser S, Vardi A, Ben-Dor S. (2014). Improving transcriptome construction in non-model organisms: integrating manual and automated gene definition in Emiliania huxleyi. *BMC Genomics* **15**: 148.
Field CB, Behrenfeld MJ, Randerson JT, Falkowski P. (1998). Primary production of the biosphere: integrating terrestrial and oceanic components. *Science* **281**: 237–240.
Fischer BB, Ledford HK, Wakao S, Huang SG, Casero D, Pellegrini M *et al.* (2012). SINGLET OXYGEN RESISTANT 1 links reactive electrophile signaling to singlet oxygen acclimation in *Chlamydomonas reinhardtii*. *Proc Natl Acad Sci USA* **109**: E1302–E1311.
Foyer CH, Noctor G. (2003). Redox sensing and signalling associated with reactive oxygen in chloroplasts, peroxisomes and mitochondria. *Physiol Plant* **119**: 355–364.
Foyer CH, Noctor G. (2005). Redox homeostasis and antioxidant signaling: a metabolic interface between stress perception and physiological responses. *Plant Cell* **17**: 1866–1875.
Foyer CH, Noctor G. (2011). Ascorbate and glutathione: the heart of the redox hub. *Plant Physiol* **155**: 2–18.
Franco R, Cidlowski JA. (2009). Apoptosis and glutathione: beyond an antioxidant. *Cell Death Differ* **16**: 1303–1314.
Fuhrman JA. (1999). Marine viruses and their biogeochemical and ecological effects. *Nature* **399**: 541–548.
George TC, Fanning SL, Fitzgerald-Bocarsly P, Fitzgeral-Bocarsly P, Medeiros RB, Highfill S *et al.* (2006). Quantitative measurement of nuclear translocation events using similarity analysis of multispectral cellular images obtained in flow. *J Immunol Methods* **311**: 117–129.
Gledhill M, Devez AA, Highfield A, Singleton C, Achterberg EP, Schroeder D. (2012). Effect of metals on the lytic cycle of the coccolithovirus, EhV86. *Front Microbiol* **3**: 155.
Go Y-M, Jones DP. (2008). Redox compartmentalization in eukaryotic cells. *Biochim Biophys Acta* **1780**: 1273–1290.
Gon S, Faulkner M, Beckwith J. (2006). In vivo requirement for glutaredoxins and thioredoxins in the reduction of the ribonucleotide reductases of *Escherichia coli*. *Antioxidants Redox Signal* **8**: 735–742.
Graff van Creveld S, Rosenwasser S, Schatz D, Koren I, Vardi A. (2014). Early perturbation in mitochondria redox homeostasis in response to environmental stress predicts cell fate in diatoms. *ISME J* **9**: 385–395.
Halliwell B, Gutteridge J. (1986). Oxygen free radicals and iron in relation to biology and medicine: some

problems and concepts. *Arch Biochem Biophys* **246**: 501–514.
Halliwell B. (2006). Reactive species and antioxidants. Redox biology is a fundamental theme of aerobic life. *Plant Physiol* **141**: 312–322.
Hatton AD, Darroch L, Malin G. (2004). The role of dimethylsulphoxide in the marine biogeochemical cycle of dimethylsulphide. *Oceanogr Mar Biol an Annu Rev* **42**: 29–56.
Holligan P, Viollier M, Harbour D. (1983). Satellite and ship studies of coccolithophore production along a continental shelf edge. *Nature* **304**: 339–342.
Janknegt PJ, van de Poll WH, Visser RJW, Rijstenbil JW, Buma AGJ. (2008). Oxidative stress responses in the marine antarctic diatom *Chaetoceros brevis* (Bacillariophyceae) during photoacclimation. *J Phycol* **44**: 957–966.
Kang M, Duncan G, Kuszynski C, Oyler G, Zheng J, Becker DF *et al.* (2014). Chlorovirus PBCV-1 encodes an active copper-zinc superoxide dismutase. *J Virol* **88**: 12541–12550.
Keller MD, Selvin RC, Claus W, Guillard RRL. (1987). Media for the culture of oceanic ultraphytoplankton. *J Phycol* **23**: 633–638.
Kimmance S, Allen MJ, Pagarete A, Martínez Martínez J, Wilson WH. (2014). Reduction in photosystem II efficiency during a virus-controlled *Emiliania huxleyi* bloom. *Mar Ecol Prog Ser* **495**: 65–76.
Kranner I, Birtić S, Anderson KM, Pritchard HW. (2006). Glutathione half-cell reduction potential: a universal stress marker and modulator of programmed cell death? *Free Radic Biol Med* **40**: 2155–2165.
Lardy B, Bof M, Aubry L, Paclet MH, Morel F, Satre M *et al.* (2005). NADPH oxidase homologs are required for normal cell differentiation and morphogenesis in *Dictyostelium discoideum*. *Biochim Biophys Acta* **1744**: 199–212.
Lehahn Y, Koren I, Schatz D, Frada M, Sheyn U, Boss E *et al.* (2014). Decoupling physical from biological processes to assess the impact of viruses on a mesoscale algal bloom. *Curr Biol* **24**: 1–6.
Li Z, Wakao S, Fischer BB, Niyogi KK. (2009). Sensing and responding to excess light. *Annu Rev Plant Biol* **60**: 239–260.
Liang H, Yao N, Song JT, Luo S, Lu H, Greenberg JT. (2003). Ceramides modulate programmed cell death in plants service ceramides modulate programmed cell death in plants. *Genes Dev* **17**: 2636–2641.
Lindell D, Jaffe JD, Johnson ZI, Church GM, Chisholm SW. (2005). Photosynthesis genes in marine viruses yield proteins during host infection. *Nature* **438**: 86–89.
Llewellyn CA, Evans C, Airs RL, Cook I, Bale N, Wilson WH. (2007). The response of carotenoids and chlorophylls during virus infection of *Emiliania huxleyi* (Prymnesiophyceae). *J Exp Mar Bio Ecol* **344**: 101–112.
Love AJ, Yun BW, Laval V, Loake GJ, Milner JJ. (2005). Cauliflower mosaic virus, a compatible pathogen of *Arabidopsis*, engages three distinct defense-signaling pathways and activates rapid systemic generation of reactive oxygen species. *Plant Physiol* **139**: 935–948.
Ma Q, Cavallin LE, Leung HJ, Chiozzini C, Goldschmidt-Clermont PJ, Mesri EA. (2013). A role for virally induced reactive oxygen species in Kaposi's sarcoma herpesvirus tumorigenesis. *Antioxidants Redox Signal* **18**: 80–90.
Martínez Martínez J, Poulton NJ, Stepanauskas R, Sieracki ME, Wilson WH. (2011). Targeted sorting of single virus-infected cells of the coccolithophore *Emiliania huxleyi*. *PLoS One* **6**: e22520.
McLachlan DH, Underwood GJC, Taylor AR, Brownlee C. (2012). Calcium release from intracellular stores is necessary for the photophobic response in the benthic diatom *Navicula Perminuta* (Bacillariophyceae). *J Phycol* **48**: 675–681.
Mittler R, Vanderauwera S, Gollery M, Van Breusegem F. (2004). Reactive oxygen gene network of plants. *Trends Plant Sci* **9**: 490–498.
Mittler R, Vanderauwera S, Suzuki N, Miller G, Tognetti VB, Vandepoele K *et al.* (2011). ROS signaling: the new wave? *Trends Plant Sci* **16**: 300–309.
Mittler R. (2002). Oxidative stress, antioxidants and stress tolerance. *Trends Plant Sci* **7**: 405–410.
Montsant A, Allen AE, Coesel S, De Martino A, Falciatore A, Mangogna M *et al.* (2007). Identification and comparative genomic analysis of signaling and regulatory components in the diatom *Thalassiosira pseudonana*. *J Phycol* **43**: 585–604.
Murik O, Elboher A, Kaplan A. (2014). Dehydroascorbate: a possible surveillance molecule of oxidative stress and programmed cell death in the green alga Chlamydomonas reinhardtii. *New Phytol* **202**: 471–484.
Murik O, Kaplan A. (2009). Paradoxically, prior acquisition of antioxidant activity enhances oxidative stress-induced cell death. *Environ Microbiol* **11**: 2301–2309.
Noctor G, Foyer CH. (1998). Ascorbate and glutathione: keeping active oxygen under control. *Annu Rev Plant Physiol Plant Mol Biol* **49**: 249–279.
Owusu-Ansah E, Banerjee U. (2009). Reactive oxygen species prime *Drosophila* haematopoietic progenitors for differentiation. *Nature* **461**: 537–541.
Pagarete A, Allen MJ, Wilson WH, Kimmance SA, De Vargas C. (2009). Host-virus shift of the sphingolipid pathway along an *Emiliania huxleyi* bloom: survival of the fattest. *Environ Microbiol* **11**: 2840–2848.
Perl A, Banki K. (2000). Genetic and metabolic control of the mitochondrial transmembrane potential and reactive oxygen intermediate production in HIV disease. *Antioxidants Redox Signal* **2**: 551–573.
Pettus BJ, Chalfant CE, Hannun YA. (2002). Ceramide in apoptosis: an overview and current perspectives. *Biochim Biophys Acta - Mol Cell Biol Lipids* **1585**: 114–125.
Potapovich MV, Metelitza DI, Shadyro OI. (2012). Antioxidant activity of hydroxy derivatives of coumarin. *Appl Biochem Microbiol* **48**: 250–256.
Queval G, Noctor G. (2007). A plate reader method for the measurement of NAD, NADP, glutathione, and ascorbate in tissue extracts: application to redox profiling during *Arabidopsis* rosette development. *Anal Biochem* **363**: 58–69.
Read BA, Kegel J, Klute MJ, Kuo A, Lefebvre SC, Maumus F *et al.* (2013). Pan genome of the phytoplankton *Emiliania* underpins its global distribution. *Nature* **499**: 209–213.
Rijstenbil JW. (2002). Assessment of oxidative stress in the planktonic diatom *Thalassiosira pseudonana* in response to UVA and UVB radiation. *J Plankton Res* **24**: 1277–1288.
Rohwer F, Thurber RV. (2009). Viruses manipulate the marine environment. *Nature* **459**: 207–212.
Rosenwasser S, Mausz MA, Schatz D, Sheyn U, Malitsky S, Aharoni A *et al.* (2014). Rewiring host lipid metabolism by large viruses determines the fate of *Emiliania*

huxleyi, a bloom-forming alga in the ocean. *Plant Cell* **26**: 2689–2707.

Rost B, Riebesell U. (2004). Coccolithophores and the biological pump: responses to environmental changes. In: Thierstein HR, Young YR (eds), *Coccolithophores: From Molecular Processes to Global Impact*. Springer: New York, NY, USA, pp 99–125.

Schatz D, Shemi A, Rosenwasser S, Sabanay H, Wolf SG, Ben-Dor S *et al.* (2014). Hijacking of an autophagy like process is critical for the life cycle of a DNA virus infecting oceanic algal blooms. *New Phytol* **204**: 854–863.

Schroeder D, Oke J, Malin G, Wilson WH. (2002). Coccolithovirus (Phycodnaviridae): characterisation of a new large dsDNA algal virus that infects *Emiliana huxleyi*. *Arch Virol* **147**: 1685–1698.

Shao H, Chu L, Shao M, Jaleel CA, Mi H. (2008). Higher plant antioxidants and redox signaling under environmental stresses. *C R Biol* **331**: 433–441.

Sharon I, Alperovitch A, Rohwer F, Haynes M, Glaser F, Atamna-Ismaeel N *et al.* (2009). Photosystem I gene cassettes are present in marine virus genomes. *Nature* **461**: 258–262.

Siddique S, Matera C, Radakovic ZS, Shamim Hasan M, Gutbrod P, Rozanska E *et al.* (2014). Parasitic worms stimulate host NADPH oxidases to produce reactive oxygen species that limit plant cell death and promote infection. *Sci Signal* **7**: ra33.

Sirois J, Miller R. (1972). The mechanism of the scopoletin-induced inhibition of the peroxidase catalyzed degradation of indole-3-acetate. *Plant Physiol* **49**: 1012–1018.

Sukenik A, Eshkol R, Livne A. (2002). Inhibition of growth and photosynthesis of the dinoflagellate *Peridinium gatunense* by *Microcystis* sp. (cyanobacteria): a novel allelopathic mechanism. *Limnol Oceanogr* **47**: 1656–1663.

Suttle CA. (2005). Viruses in the sea. *Nature* **437**: 356–361.

Suttle CA. (2007). Marine viruses-major players in the global ecosystem. *Nat Rev Microbiol* **5**: 801–812.

Taylor AR. (2009). A fast Na+/Ca2+-based action potential in a marine diatom. *PLoS One* **4**: e4966.

Thamatrakoln K, Korenovska O, Niheu AK, Bidle KD. (2012). Whole-genome expression analysis reveals a role for death-related genes in stress acclimation of the diatom *Thalassiosira pseudonana*. *Environ Microbiol* **14**: 67–81.

Tietze F. (1969). Enzymic method for quantitative determination of nanogram amounts of total and oxidized glutathione: applications to mammalian blood and other tissues. *Anal Biochem* **27**: 502–522.

Tsukagoshi H, Busch W, Benfey PN. (2010). Transcriptional regulation of ROS controls transition from proliferation to differentiation in the root. *Cell* **143**: 606–616.

Tyrrell T, Merico A. (2004). *Emiliania huxleyi*: bloom observations and the conditions that induce them. In: Thierstein HR, Young YR (eds), *Coccolithophores: From Molecular Processes to global impact*. Springer: New York, NY, USA, pp 585–604.

Van Breusegem F, Dat JF. (2006). Reactive oxygen species in plant cell death. *Plant Physiol* **141**: 384–390.

Vardi A, Berman-Frank I, Rozenberg T, Hadas O, Kaplan A, Levine A. (1999). Programmed cell death of the dinoflagellate *Peridinium gatunense* is mediated by CO2 limitation and oxidative stress. *Curr Biol* **9**: 1061–1064.

Vardi A, Eisenstadt D, Murik O, Berman-Frank I, Zohary T, Levine A *et al.* (2007). Synchronization of cell death in a dinoflagellate population is mediated by an excreted thiol protease. *Environ Microbiol* **9**: 360–369.

Vardi A, Formiggini F, Casotti R, De Martino A, Ribalet F, Miralto A *et al.* (2006). A stress surveillance system based on calcium and nitric oxide in marine diatoms. *PLoS Biol* **4**: 411–419.

Vardi A, Haramaty L, Van Mooy BA, Fredricks HF, Kimmance SA, Larsen A *et al.* (2012). Host-virus dynamics and subcellular controls of cell fate in a natural coccolithophore population. *Proc Natl Acad Sci USA* **109**: 19327–19332.

Vardi A, Schatz D, Beeri K, Motro U, Sukenik A, Levine A *et al.* (2002). Dinoflagellate-cyanobacterium communication may determine the composition of phytoplankton assemblage in a mesotrophic lake. *Curr Biol* **12**: 1767–1772.

Vardi A, Van Mooy BA, Fredricks HF, Popendorf KJ, Ossolinski JE, Haramaty L *et al.* (2009). Viral glycosphingolipids induce lytic infection and cell death in marine phytoplankton. *Science* **326**: 861–865.

Veal EA, Day AM, Morgan BA. (2007). Hydrogen peroxide sensing and signaling. *Mol Cell* **26**: 1–14.

Wilhelm S, Suttle CA. (1999). Viruses and nutrient cycles in the sea viruses play critical roles in the structure and function of aquatic food webs. *Bioscience* **49**: 781–788.

Wilson WH, Schroeder DC, Allen MJ, Holden MTG, Parkhill J, Barrell BG *et al.* (2005). Complete genome sequence and lytic phase transcription profile of a Coccolithovirus. *Science* **309**: 1090–1092.

Wilson WH, Tarran GA, Schroeder D, Cox M, Oke J, Malin G. (2002). Isolation of viruses responsible for the demise of an *Emiliania huxleyi* bloom in the English Channel. *J Mar Biol Assoc UK* **82**: 369–377.

Winter C, Bouvier T, Weinbauer MG, Thingstad TF. (2010). Trade-offs between competition and defense specialists among unicellular planktonic organisms: the 'killing the winner' hypothesis revisited. *Microbiol Mol Biol Rev* **74**: 42–57.

Ye F, Zhou F, Bedolla RG, Jones T, Lei X, Kang T *et al.* (2011). Reactive oxygen species hydrogen peroxide mediates Kaposi's sarcoma-associated herpesvirus reactivation from latency. *PLoS Pathog* **7**: e1002054.

Yoda H, Yamaguchi Y, Sano H. (2003). Induction of hypersensitive cell death by hydrogen peroxide produced through polyamine degradation in tobacco plants. *Plant Physiol* **132**: 1973–1981.

Zhang R, Kim S, Kang K, Piao M, Ko D, Wang Z *et al.* (2008). Protective effect of esculetin against oxidative stress-induced cell damage via scavenging reactive oxygen species. *Acta Pharmacol Sin* **29**: 1319–1326.

Supplementary Information accompanies this paper on The ISME Journal website (http://www.nature.com/ismej)